

Error filtration from optimized quantum circuit interference

Aaqib Ali,^{1, 2} Giovanni Scala,^{3, 2} and Cosmo Lupo^{1, 3, 2}

¹*Dipartimento Interateneo di Fisica, Università di Bari, 70126 Bari, Italy*

²*INFN, Sezione di Bari, 70126 Bari, Italy*

³*Dipartimento Interateneo di Fisica, Politecnico di Bari, 70126 Bari, Italy*

We develop an optimized hardware strategy to mitigate errors in a noisy qubit. Our scheme builds on the physical principle of error filtration and exploits auxiliary qubits. Both signal and ancillas are subject to local noise, yet constructive interference (and in some cases post-selection) allows us to reduce the level of noise in the signal qubit. Seeking for the optimal unitary that makes the qubits interfere in the most effective way, we start with a set of universal gates and proceed by optimizing suitable functionals by gradient descent or stochastic approximation. We benchmark our approach against a number of figure of merits that correspond to different applications, including entanglement fidelity, quantum Fisher information (for applications in quantum sensing), and CHSH value (for applications in tests of non-locality and quantum cryptography), with one, two, and three ancillary qubits. With one and two ancillas we also provide explicit expressions from an ansatz for an optimal unitary.

I. INTRODUCTION

Quantum information science leverages quantum mechanics to collect, convey, and process information, opening up capabilities beyond the boundaries of classical physics [1]. It supports the development of quantum computing, which promises to outperform traditional computers in solving particular problems of great interest [2–7]. In the field of metrology and sensing, quantum effects may significantly boost measurement precision, benefiting various disciplines, from optical imaging to astronomy and magnetometry [8–13]. In the context of communication, quantum non-locality, witnessed and quantified by the violation of suitable Bell inequalities, paves the way to device-independent quantum key distribution, which arguably allows for the highest level of cybersecurity [14–16] (for an overview on the topic see Refs. [17, 18]).

The main challenge in quantum information processing is maintaining quantum coherence by correcting or mitigating the effects of qubit-environment interactions. In the ongoing phase of development of quantum technologies, dubbed Noisy Intermediate-Scale Quantum (NISQ) era [19], there is a strong focus on developing and implementing advanced error mitigation strategies for small-to-medium scale quantum devices [20–26]. These methods are crucial for enhancing the reliability and accuracy of quantum operations, even if large-scale fault-tolerant architectures are not yet available.

In this work we develop a hardware approach to error mitigation based on the physical phenomenon of error filtration [27, 28]. Our scheme makes use of one or more ancillary qubits. The signal qubit is first coupled with the ancillas through some (to-be-optimized) unitary U . After this encoding procedure, both the signal and auxiliary qubits are subject to local, independent noise. For decoding, the inverse unitary is applied. By carefully choosing the encoding unitary U , one may exploit constructive and destructive interference in order to reduce the cumulative noise in the signal qubit, at the expense of

augmented noise in the ancillas. Depending on the application, and hence on the figure of merit, we also consider the post-selected state of the signal qubit conditioned on a measurement of the ancillas.

Other authors have explored error filtration as a means to reduce errors in quantum information processing. Previous works have considered applications in optics, where the light field is demultiplexed and recombined through a pair of conjugate interferometers [29, 30]. By contrast, Refs. [31–33] applied error filtration to quantum information encoded in qubits, given a noisy gate, where the constructive interference is implemented with a particular quantum circuit design. Lee *et al.* [31] exploited a circuit that implemented a superposition of trajectories, with the noisy gate applied sequentially to the target qubit, assisted by control-SWAP gates, ancillary and control qubits. Miguel-Ramiro *et al.* [32, 33] considered a circuital simulation of the superposition of causal orders (both in the gate-based and in the measurement-based computational model), with parallel application of the noisy gate, also with the assistance of control-SWAP gates and ancillary and control qubits

Here our goal is to find the optimal encoding and decoding unitary that, with the help of a small number of ancillas (we use from one up to three auxiliary qubits) can most efficiently mitigate dephasing or depolarizing noise in the signal qubit. Therefore, instead of fixing the form of the circuit, we consider a parameterized family of universal gates and search for the optimal one. Unlike Refs. [31–33] our main focus is on shielding quantum information instead of processing it, therefore our results mostly apply to error-mitigation in a noisy quantum memory or through a noisy quantum channel. Unlike previous works, our scheme retains robustness when noise affects with equal strength both signal and ancillary qubits, though we assume noiseless pre and post-processing operations. Our approach is applied across a variety of settings, each corresponding to a different figure of merit. For computation and general quantum information processing we focus on the entanglement fidelity [1]. For fun-

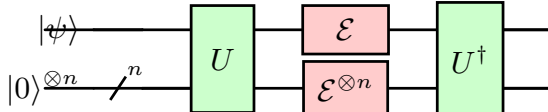


FIG. 1. General scheme of our hardware-based error mitigation approach, depicted for the case of one signal qubit and n ancillary qubits. The signal qubit is initialized into a generic state $|\psi\rangle$, and the ancillas in the computational basis state $|0\rangle^{\otimes n}$. The encoding qubit unitary U is applied to signal and ancillas before the action of the local noisy channel \mathcal{E} . Each qubit is subject to statistically independent and identically distributed errors. Following the noisy channel, the inverse unitary U^\dagger is applied for decoding.

damental tests of non-locality and for quantum cryptography the CHSH inequality is considered [34–38]. Finally, for applications in sensing and metrology we examine the quantum Fisher information [39].

The paper proceeds as follows. In Section II we introduce our approach, a suitable parameterization for the encoding and decoding unitary, and the noise model. The results of the numerical optimization, and an ansatz for the optimal encoding, are presented in Section III. Conclusions and an overview of future development are presented in Section IV.

II. QUANTUM INTERFERENCE FROM UNIVERSAL UNITARY GATES

In our model, we assume that the signal qubits are affected by noise. To mitigate these errors we consider one or more ancillary qubits, which are mixed with the signal qubits through a encoding unitary U . We assume that this unitary is implemented without errors. The parameterization of the unitary is described in Section II A. To model the errors, we explicitly consider and discuss the case of a noisy channel \mathcal{E} that is either a dephasing or a depolarizing channel, as reviewed in Section II B.

Our hardware scheme for error mitigation is depicted in Fig. 1, for the case of one signal qubit and n ancillary qubits. The signal qubit is initialized in a generic state $|\psi\rangle$. The ancillas are initialized in the computational basis state $|0\rangle^{\otimes n}$. After the application of the encoding unitary U , the qubits are affected by local errors, which we assume statistically independent and identically distributed. These errors may be due to an imperfect storage into a quantum memory, or to transmission through a noisy communication line. Following the application of the noise, the inverse unitary U^\dagger is applied in order to decode the quantum information initially encoded in signal and ancillary qubits. Finally, and depending on the particular use case of the mitigation scheme, we may apply a measurement to the ancillary qubits and consider the conditional state of the signal qubit.

Unlike Refs. [31–33], we do not assume a particular form for the circuit that implements the unitary U . In-

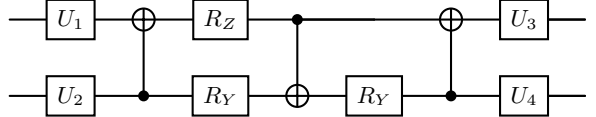


FIG. 2. Construction of a two-qubit unitary gate from four single-qubit gates $U_1, U_2, U_3, U_4 \in \text{U}(2)$, three C-NOT gates, two rotations along the y -axis, and one along the z -axis [50].

stead, we keep it generic and search for the one that allows for optimal performance. To achieve this goal with n ancillary qubits, we need to parameterize the set of unitary matrices acting on $n + 1$ qubits.

A. Universal unitary gates

Universal unitary gates are foundational components in the architecture of quantum computing. They have the capacity to approximate any quantum operation, which is a crucial property for devising quantum algorithms that can tackle a broad spectrum of computational challenges.

Our approach to constructing unitary transformations relies on a systematic decomposition into basic rotational and universal gates, such as $R_X = e^{-i\theta\sigma_x/2}$, $R_Y = e^{-i\phi\sigma_y/2}$, and $R_Z = e^{-i\gamma\sigma_z/2}$, where σ_x , σ_y , σ_z are the Pauli matrices. The literature offers multiple decomposition strategies, including Givens rotations and sine-cosine decompositions, which provide a structured methodology for simplifying complex quantum gates into more manageable subunits (see Refs. [40–48]).

For the specific task of constructing a two-qubit unitary transformation (i.e. for an error mitigation scheme with $n = 1$ ancillary qubit), we adopt the circuit architecture described in Ref. [49]. Figure 2 illustrates how a generic two-qubit unitary gate $U \in \text{U}(2^2)$ can be synthesized from single-qubit gates and the two-qubit gate C-NOT.

To expand this construction to more qubits (number of ancillas $n \geq 2$), we employ the Quantum Shannon Decomposition (QSD) described in Ref. [50]. The QSD method recursively allows for the implementation of an arbitrary $(n + 1)$ -qubit unitary operation through a sequence of multiplexed rotations and n -qubit unitaries, arranged in a specific circuit configuration as depicted in Figs. 3–5. However, while the QSD recursion is adaptable to circuits with any number of qubits, it does increase the number of required C-NOT gates. This trade-off is managed by recursively applying the decomposition until the circuit simplifies to two-qubit gates, after which we used minimal decomposition as described in Ref. [50].

Given such decomposition and parameterization of a generic circuit, we can define and solve the problem of finding the parameters that maximize a suitable figure of merit that characterizes the performance of the error mitigation scheme in Fig. 1 with one or more ancillas.

To achieve this, we have used PennyLane [51], a

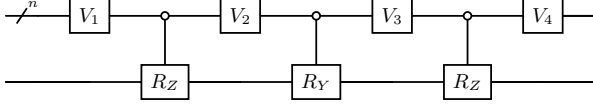


FIG. 3. Quantum Shannon Decomposition for constructing $U \in \mathrm{U}(2^{n+1})$ involving recursive application of $V_1, V_2, V_3, V_4 \in \mathrm{U}(2^n)$ and multiplexed rotations [50]. The recursive definition of the multiplexed rotation is shown in Fig. 4.

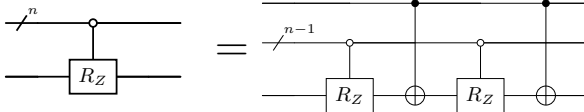


FIG. 4. By recursively applying the decomposition shown in the picture, one can decompose any multiplexed rotation into elementary gates [50].

Python-based library that proved most effective for our needs. Utilizing PennyLane, we were able to finely tune and determine the optimal values for the gate parameters, thereby enhancing the overall performance of our quantum circuits. Such a comprehensive approach not only underscores the versatility of universal unitary gates in enhancing the practicality and effectiveness of quantum algorithms but also highlights the precision with which these complex operations can be modelled and implemented.

B. Noise models

In the error mitigation circuit depicted in Fig. 1 we assume a consistent noisy channel affecting both signal and ancillary qubits. As an example, we explore two prevalent models of quantum noise: the *dephasing channel* and the *depolarizing channel*.

The dephasing channel, denoted as \mathcal{E}_φ , primarily affects the relative phase between elements of the computational basis. It is represented by the Kraus operators:

$$\sqrt{p_\varphi} \sigma_0, \sqrt{1 - p_\varphi} \sigma_z, \quad (1)$$

where σ_0 denotes the identity matrix. This channel preserves the states in the computational basis states but introduces phase errors. The transformation induced by this channel on an input state $|\psi\rangle$ is:

$$\mathcal{E}_\varphi (|\psi\rangle\langle\psi|) = q_\varphi |\psi\rangle\langle\psi| + (1 - q_\varphi) \tau_\psi, \quad (2)$$

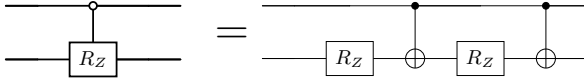


FIG. 5. For $n = 1$, the multiplexed rotation is defined by combining to C-NOT gates and two single-qubit rotations. Note that in general the two single-qubit rotations have different angles [50].

where $q_\varphi = 2p_\varphi - 1$ and

$$\tau_\psi = \frac{|\psi\rangle\langle\psi| + \sigma_z|\psi\rangle\langle\psi|\sigma_z}{2} \quad (3)$$

is the state with phase information erased.

The depolarizing channel, denoted as \mathcal{E}_r , models the loss of quantum information without bias towards any specific basis. Its effect on a quantum state can be described using the Kraus operators:

$$\sqrt{p_r} \sigma_0, \sqrt{\frac{1 - p_r}{3}} \sigma_x, \sqrt{\frac{1 - p_r}{3}} \sigma_y, \sqrt{\frac{1 - p_r}{3}} \sigma_z. \quad (4)$$

The channel transforms any input state towards the maximally mixed state $\sigma_0/2$. The action on a pure state $|\psi\rangle$ is

$$\mathcal{E}_r (|\psi\rangle\langle\psi|) = q_r |\psi\rangle\langle\psi| + (1 - q_r) \frac{\sigma_0}{2}, \quad (5)$$

where the parameter $q_r = (4p_r - 1)/3$ quantifies the probability that the input state remains unchanged, and $(1 - q_r)$ is the probability that it is replaced by the maximally mixed state.

III. NUMERICAL RESULTS AND THEORETICAL INSIGHTS

The primary objective of this study is to demonstrate and quantitatively assess the effectiveness of our error mitigation scheme. We achieve this by utilizing a functional \mathfrak{F} computed on the output state. Depending on the particular application, the functional identifies a suitable metric for quantifying quantum information, e.g., the entanglement fidelity, the CHSH functional, or the quantum Fisher information.

Given an input state for the signal qubit, and having initialized the ancillary qubits in the state $|0\rangle$, the functional depends on the unitary $U \in \mathrm{U}(2^{n+1})$ that mixes the signal qubit with n ancillas. Specifically, we consider the following optimization:

$$\mathfrak{F}_n = \max_{U \in \mathrm{U}(2^{n+1})} \mathfrak{F}[U]. \quad (6)$$

Since $\mathrm{U}(2^{n+1})$ is a subgroup of $\mathrm{U}(2^{n+2})$, we have $\mathfrak{F}_{n+1} \geq \mathfrak{F}_n$, as well as $\mathfrak{F}_n \geq \mathfrak{F}_0$, where $n = 0$ corresponds to the functional evaluation without application of the error mitigation strategy. In theory, increasing the number of ancillas would improve the value of the chosen figure of merit. However, in experimental scenarios, this is no longer accurate due to the additional noise introduced by the increased complexity of the quantum circuit that implements U .

A. Optimization scheme

The parameterization of a generic special on $n + 1$ qubits requires 2^{2n+2} parameters (including the global

phase that can be neglected); thus, for one, two, and three ancillas, we need at least 16, 64, and 256 parameters, respectively. These parameters can be defined using the decomposition discussed in Section II A. While optimizing a circuit with one ancilla is relatively straightforward, the number of parameters increases exponentially with each additional ancilla, necessitating substantial computational resources and sophisticated optimization strategies.

For high computing power, we utilized the ReCaS-Bari Data Center¹. This HPC cluster runs the jobs in parallel, providing the necessary computational resources to handle the large number of parameters efficiently. In machine learning, it is a common practice to optimize over a large number of parameters, and we leverage this knowledge in our approach to optimize quantum circuits. We employ **PennyLane**, a machine learning-oriented Python library, to achieve optimal parameter settings for our quantum circuit. We design cost functions based on specific performance metrics.

For optimization, gradient descent is our primary tool, favored for its efficiency in navigating complex parameter spaces. To avoid the common challenge of local minima, we also incorporate gradient-free optimizers. We determine the number of iterations by monitoring convergence trends to ensure the parameters evolve towards a stable and effective solution. To confirm the stability and reliability of our optimized circuit, we conduct multiple optimization runs with different random seeds. This helps verify the consistency of the outcomes and identify the most dependable parameter settings. Our structured optimization process is designed to systematically refine the parameters of our quantum circuit, thus enhancing both its performance and reliability in quantum computing tasks.

B. Entanglement fidelity

The entanglement fidelity quantifies the ability of a physical transformation to preserve entanglement with a reference system. In order to use this functional as a figure of merit to assess our error mitigation scheme we need to introduce a reference qubit, in such a way that the initial state of signal (S) and reference (R) is maximally entangled. Without loss of generality we consider

$$|\Phi^+\rangle = \frac{1}{\sqrt{2}} (|0\rangle_R |0\rangle_S + |1\rangle_R |1\rangle_S). \quad (7)$$

The scheme is depicted in Fig. 6. At the output, we consider the joint state of the signal and reference conditioned on measuring the n ancillary qubits in the computation state $|0\rangle^{\otimes n}$. This state is represented by the

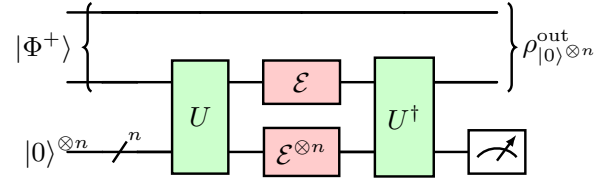


FIG. 6. Error mitigation scheme designed to maximize the entanglement fidelity. A maximally-entangled two-qubit state $|\Phi^+\rangle$ is initially prepared for the reference and signal qubits. In pre-processing, the signal interacts with n ancillary qubits through the encoding unitary U . Signal and ancillary qubits are then subject to statistically independent and identically distributed errors, represented by the noisy channel \mathcal{E} . In post-processing, the inverse unitary is applied to signal and ancillary qubits, and the latter are measured in the computational basis. Here $\rho_{|0\rangle^{\otimes n}}^{\text{out}}$ denote the (not-normalized) state of the reference and signal qubits, conditioned on having measured the ancillary qubits in the state $|0\rangle^{\otimes n}$.

not-normalized density matrix $\rho_{|0\rangle^{\otimes n}}^{\text{out}}$, where the post-selection probability is given by the trace

$$P_n = \text{Tr} \rho_{|0\rangle^{\otimes n}}^{\text{out}}. \quad (8)$$

The entanglement fidelity then reads

$$\mathcal{F}_n = \frac{1}{P_n} \langle \Phi^+ | \rho_{|0\rangle^{\otimes n}}^{\text{out}} | \Phi^+ \rangle. \quad (9)$$

We have numerically optimized the entanglement fidelity over the choice of the encoding and decoding unitary, for $n = 1, 2, 3$ ancillary qubits, and evaluated the post-selection probability corresponding to maximum fidelity. The results of the numerical optimization are shown by the circle data-points in Figs. 7-8 and compared with the fidelity attainable without mitigation, which is $\mathcal{F}_0 = (1 + q_\varphi)/2$ for the dephasing channel, and $\mathcal{F}_0 = (1 + 3q_r)/4$ for the depolarizing channel (without error mitigation this is achieved deterministically, i.e. with $P_0 = 1$).

Figures 7-8 show the trade-off arising when introducing ancillary qubits: with more ancillas the fidelity is enhanced but at the cost of reducing the success probability. We also note that the scheme works better for dephasing rather than depolarising noise. This is in line with the observations of Refs. [32, 33] and corresponds to the fact that the depolarizing channel has higher Kraus rank (i.e., the number of Kraus operators) than the dephasing channel.

C. Ansatz for the optimal unitary

In this Section we propose explicit forms for the encoding and decoding unitary that match the results of the numerical optimization.

Let us first consider the case of $n = 1$ auxiliary qubit. We note that, since the ancilla is initialized in $|0\rangle$, it is sufficient to consider the action of the encoding unitary on

¹ <https://www.recas-bari.it/index.php/en/>

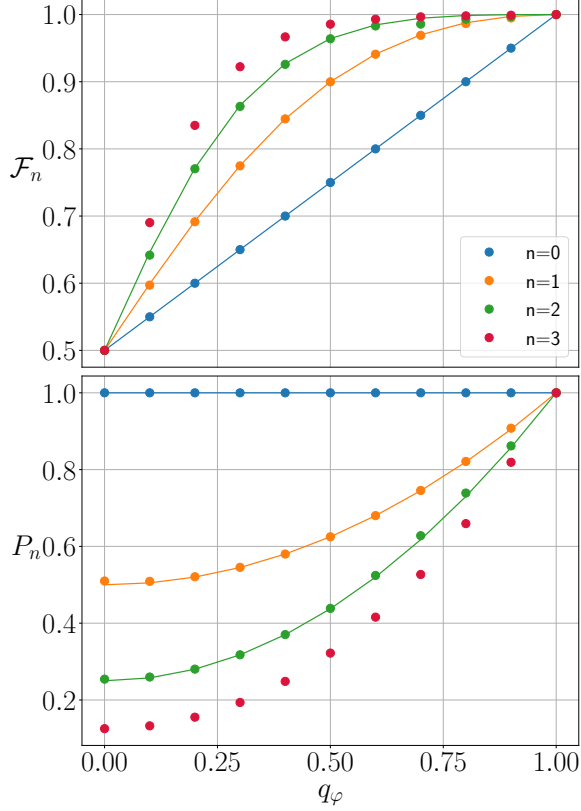


FIG. 7. Entanglement Fidelity (upper panel) and success probability (lower panel) plotted vs the noise parameter $q_\varphi \in [0, 1]$ for *dephasing channel*, as in Eq. (2) with $n = 0, 1, 2, 3$ ancillary qubits (see the legend). Dots represent the numerical results, solid lines are used to denote the analytical results from Eqs. (20), (22), (27), (28).

the states $|0\rangle_S|0\rangle_A$ and $|1\rangle_S|0\rangle_A$, where A labels the ancillary qubits. Our ansatz for the optimal encoding follows directly from the optical error filtration scheme [27, 30]. We assume that the two states $|0\rangle_S|0\rangle_A$ and $|1\rangle_S|0\rangle_A$ are mapped into two Bell states, for example

$$|0\rangle_S|0\rangle_A \xrightarrow{U} U|0\rangle_S|0\rangle_A = \frac{|00\rangle + |11\rangle}{\sqrt{2}} = |\Phi^+\rangle_{SA}, \quad (10)$$

$$|1\rangle_S|0\rangle_A \xrightarrow{U} U|1\rangle_S|0\rangle_A = \frac{|10\rangle + |01\rangle}{\sqrt{2}} = |\Psi^+\rangle_{SA}. \quad (11)$$

This encoding can be implemented by different choices for the unitary U . For example, a possible choice is the one that maps the computation basis into the Bell basis.

With this encoding rule, the initial state $|\Phi^+\rangle$ of refer-

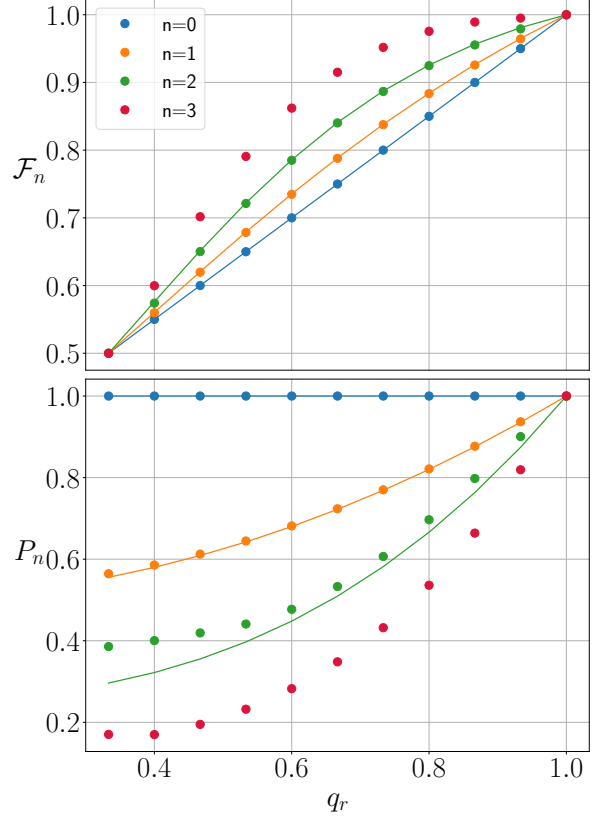


FIG. 8. Entanglement Fidelity (upper panel) and success probability (lower panel) plotted vs the noise parameter $q_r \in [1/3, 1]$ for *depolarizing channel*, as in Eq. (5), with $n = 0, 1, 2, 3$ ancillary qubits (see the legend). Dots represent the numerical results, solid lines are used to denote the analytical results obtained in Eqs. (23)-(24) and (31)-(32).

ence and signal qubits in Eq. (7) is transformed as follows:

$$|\Phi^+\rangle_{RS}|0\rangle_A = \frac{1}{\sqrt{2}} (|0\rangle_R|0\rangle_S|0\rangle_A + |1\rangle_R|1\rangle_S|0\rangle_A) \quad (12)$$

$$\xrightarrow{U} \frac{1}{\sqrt{2}} (|0\rangle_R U|0\rangle_S|0\rangle_A + |1\rangle_R U|1\rangle_S|0\rangle_A) \quad (13)$$

$$= \frac{1}{\sqrt{2}} (|0\rangle_R |\Phi^+\rangle_{SA} + |1\rangle_R |\Psi^+\rangle_{SA}) \quad (14)$$

$$= \frac{1}{2} (|000\rangle + |011\rangle + |110\rangle + |101\rangle), \quad (15)$$

where in the last line we have dropped the labels R, S, A .

Let us look in more detail to the case of dephasing channel. The action of this noise to each qubit can be described as the application of a random phase in the computation basis, expressed by the operator $e^{i\theta_j|1\rangle_j\langle 1|}$ applied on the j -th qubit, where θ_j is a random variable. Its probability density distribution $\mu(\theta)$ determines the dephasing parameter q_φ as

$$q_\varphi = \int d\theta \mu(\theta) \cos \theta. \quad (16)$$

The application of a random phase to the above state in Eq. (15) yields (recall that the reference is not subject to noise)

$$\frac{1}{2} (|000\rangle + e^{i\theta_1+i\theta_2}|011\rangle + e^{i\theta_1}|110\rangle + e^{i\theta_2}|101\rangle) . \quad (17)$$

The application of the inverse circuit (mapping the Bell basis back into the computation basis), followed by the projection onto the state $|0\rangle$ of the ancilla, yields

$$|\psi_{\theta_1\theta_2}\rangle = \frac{1}{\sqrt{2}} \left(\frac{1+e^{i\theta_1+i\theta_2}}{2} |00\rangle + \frac{e^{i\theta_1}+e^{i\theta_2}}{2} |11\rangle \right) . \quad (18)$$

The above state is not normalized. To obtain the post-selection probability we need to average its squared modulus over the noise realizations, obtaining

$$P_1(q_\varphi) = \int d\theta_1 d\theta_2 \mu(\theta_1) \mu(\theta_2) \langle \psi_{\theta_1\theta_2} | \psi_{\theta_1\theta_2} \rangle \quad (19)$$

$$= (1+q_\varphi^2)/2 . \quad (20)$$

Similarly, the entanglement fidelity reads

$$\mathcal{F}_1(q_\varphi) = \frac{1}{P_1} \int d\theta_1 d\theta_2 \mu(\theta_1) \mu(\theta_2) |\langle \Phi^+ | \psi_{\theta_1\theta_2} \rangle|^2 \quad (21)$$

$$= \frac{1}{2} + \frac{q_\varphi}{1+q_\varphi^2} . \quad (22)$$

The above values of the entanglement fidelity and the success probability match the numerical results up to machine precision, see Fig. 7. A similar construction is presented in Appendix A for the case of depolarizing channel, yielding

$$P_1(q_r) = \frac{1+q_r^2}{2} , \quad (23)$$

$$\mathcal{F}_1(q_r) = \frac{1}{4} \frac{1+2q_r+5q_r^2}{1+q_r^2} , \quad (24)$$

which also match the numerical results.

In summary, for the case of one ancillary qubit, we formulate our conjecture for the optimal encoding:

Conjecture 1 *The optimal encoding for one ancilla maps the computational basis into the Bell basis.*

We now introduce an ansatz for the unitary in the case of two ancillas taking inspiration from the case of one ancilla. We note that, in a space of dimension four, an optimal encoding in the case of one ancilla was based on equally-weighted superposition of two vectors in the computational basis, see Eqs. (10),(11). We also note that these vectors have different parity. This suggests the following encoding rule with two ancillas:

$$|0\rangle_S |00\rangle_A \xrightarrow{U} |0\rangle_S |00\rangle_A = \frac{|000\rangle + |011\rangle + |101\rangle + |110\rangle}{2} , \quad (25)$$

$$|1\rangle_S |00\rangle_A \xrightarrow{U} |1\rangle_S |00\rangle_A = \frac{|001\rangle + |010\rangle + |100\rangle + |111\rangle}{2} . \quad (26)$$

In Appendix B we compute the success probability and entanglement fidelity obtained with this encoding. For dephasing noise we obtain

$$P_2(q_\varphi) = \frac{1+3q_\varphi^2}{4} , \quad (27)$$

$$\mathcal{F}_2(q_\varphi) = \frac{(q_\varphi+1)^3}{6q_\varphi^2+2} , \quad (28)$$

which match the numerical results shown in Fig. 7. More details on this are presented in Appendix B.

For depolarizing errors, a similar encoding also work, with some minus sign in the decomposition along the computational basis:

$$|0\rangle_S |00\rangle_A \xrightarrow{U} |0\rangle_S |00\rangle_A = \frac{|000\rangle + |011\rangle + |101\rangle + |110\rangle}{2} , \quad (29)$$

$$|1\rangle_S |00\rangle_A \xrightarrow{U} |1\rangle_S |00\rangle_A = \frac{|001\rangle - |010\rangle + |100\rangle - |111\rangle}{2} . \quad (30)$$

With this choice we compute

$$P_2 = \frac{1+q_r^2+2q_r^3}{4} , \quad (31)$$

$$\mathcal{F}_2 = \frac{1}{4} \frac{1+7q_r^2}{1-q_r+2q_r^2} , \quad (32)$$

which also match the numerical results for depolarizing noise, as shown in Figs. 7-8.

We thus formulate our conjecture for the optimal encoding with two ancillas:

Conjecture 2 *The optimal encoding for two ancillary qubits maps the states $|000\rangle$, $|100\rangle$ into an equally-weighted sum of computations states with given parity:*

$$|000\rangle \rightarrow \frac{|000\rangle + w_1|011\rangle + w_2|101\rangle + w_3|110\rangle}{2} , \quad (33)$$

$$|111\rangle \rightarrow \frac{|001\rangle + w_4|010\rangle + w_5|100\rangle + w_6|111\rangle}{2} , \quad (34)$$

for some choices of the coefficients such that $|w_i|^2 = 1$.

This conjecture works well for entanglement fidelity and for some of the other figures of merit, as shown in the following Sections.

D. Violation of Bell inequalities

In July 2022, three research teams had independently shown unbreakable communication via device-independent quantum key distribution [52–54]. The core principle behind this unbreakable cryptography sits on the foundation of quantum mechanics and it is obtained via a Bell-test experiment [55] in the following simplest scenario [56].

Consider a bipartite state ρ_{AB} of two qubits, shared between two distant laboratories, indicated as Alice (A) and Bob (B). In each laboratory, one out of two possible observables is measured, represented by matrices $M_{i,j}$, where

$$M_{i,j} = \begin{pmatrix} \cos \theta_{ij} & e^{-i\phi_{ij}} \sin \theta_{ij} \\ e^{i\phi_{ij}} \sin \theta_{ij} & -\cos \theta_{ij} \end{pmatrix}. \quad (35)$$

Here $i = 0, 1$ labels the sub-systems ($i = 0$ for Alice and $i = 1$ for Bob), and $j = 0, 1$ labels two possible measurement settings. The measurements are dichotomic, i.e., each has two possible outcomes $a, b \in \{-1, +1\}$. After repeated measurements, Alice and Bob can estimate the CHSH functional [56]

$$\mathcal{B} = \left| \sum_{x,y=0}^1 (-1)^{xy} \text{Tr} (M_{0,x} \otimes M_{1,y} \rho_{AB}) \right|. \quad (36)$$

According to Bell theorem, for any separable state we have $\mathcal{B} \leq 2$. However, the experimental data may violate this bound, up to $\mathcal{B} = 2\sqrt{2}$ if the state ρ_{AB} is entangled [57].

Since the violation of Bell inequalities is a signature of nonlocality monogamy and cannot be simulated by any classical means, it provides a strong guarantee of quantum correlations that, under suitable assumptions, is considered to be *device-independent* [18]. That is, this procedure does not rely on the knowledge of the internal structure of the devices used by Alice and Bob. The drawback of this approach is that experimental violation of the CHSH inequality is difficult due to the noise. For this reason we implement our error mitigation technique with the goal of maximizing the value of the Bell functional \mathcal{B} , given a noisy channel affecting the qubit en route from Alice to Bob [58].

Our model is shown in Fig. 6. First the entangled state $|\Phi^+\rangle$ is prepared locally by Alice. Along the way towards Bob's laboratory, noise is applied to the qubit (either dephasing or depolarizing noise), which in turn is mitigated with the help of n ancillary qubits and an encoding and decoding unitary U . The ancillary qubits interact with the signal qubit before the noisy channel. Signal and ancillas are subject to independent and identically distributed errors, and finally recombined with the inverse unitary U^\dagger . Consider the (not-normalized) post-selected state $\rho_{|0\rangle^{\otimes n}}^{\text{out}}$, conditioned on measuring the ancillary qubits in the computational basis state $|0\rangle^{\otimes n}$. The probability of successful error mitigation is

$$P_n = \text{Tr} \rho_{|0\rangle^{\otimes n}}^{\text{out}}, \quad (37)$$

achieving the following value for the CHSH functional

$$\mathcal{B}_n = \frac{1}{P_n} \left| \sum_{x,y=0}^1 (-1)^{xy} \text{Tr} (M_{0,x} \otimes M_{1,y} \rho_{|0\rangle^{\otimes n}}^{\text{out}}) \right|. \quad (38)$$

The above functional depends on a number of parameters. First, it depends on the parameters that determine the encoding and decoding unitary U (see Section

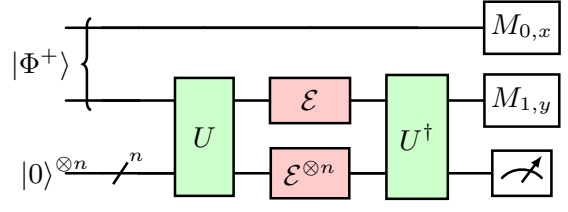


FIG. 9. Error mitigation scheme designed to maximize the violation of the CHSH inequality. A maximally-entangled two-qubit state $|\Phi^+\rangle$ is initially prepared locally in Alice laboratory. Alice keeps the first qubit in her laboratory, where in principle is stored without noise. In pre-processing, the second qubit interacts with n ancillary qubits through the encoding unitary U . The second qubit and the ancillary qubits travel towards Bob's laboratory and are subject to statistically independent and identically distributed errors, represented by the noisy channel \mathcal{E} . In Bob's laboratory, the inverse unitary is applied to the received qubits, following a measurement of the ancillary qubits in the computational basis. Alice and Bob apply the Bell test to their shared state, using local operators $M_{0,x}$ and $M_{1,y}$, conditioned on having measured the ancillary qubits in the state $|0\rangle^{\otimes n}$.

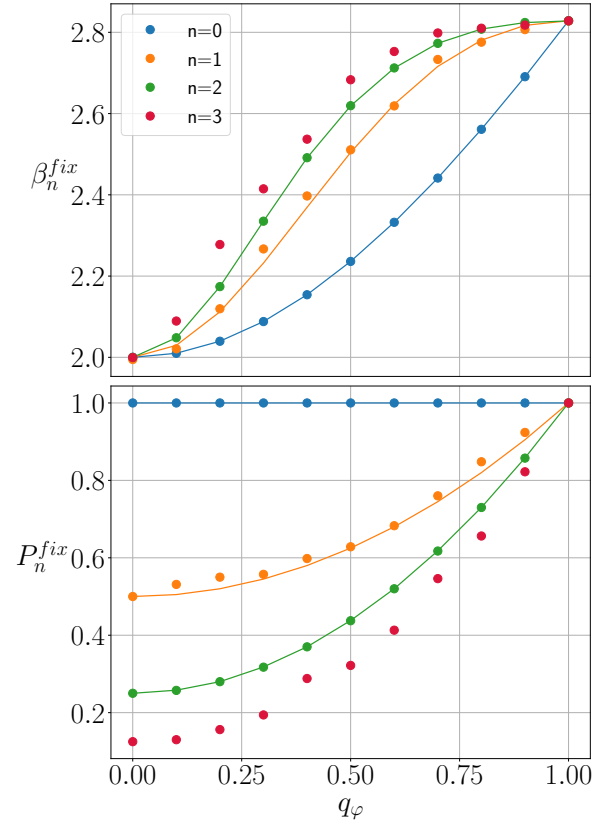


FIG. 10. Optimal CHSH value (top panel) at fixed measurement settings (see Eq. 39) and success probability (lower panel) plotted vs the noise parameter $q_\varphi \in [0, 1]$ for *dephasing channel* (see Eq. (2)) with $n = 0, 1, 2, 3$ ancillary systems (see the legend). Dots represent the numerical results, solid lines are used to denote the analytical results from Eqs. (20), (27), (51), (52).

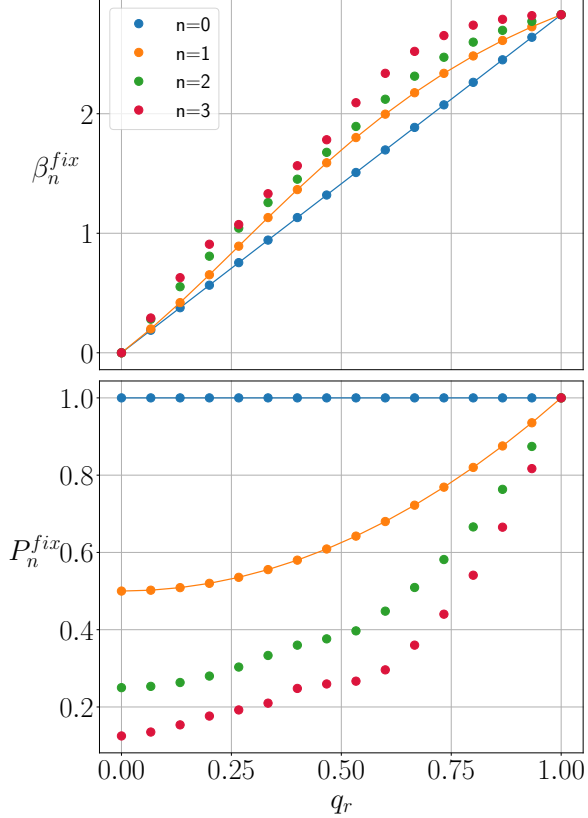


FIG. 11. Optimal CHSH value (top panel) at fixed measurement settings of (see Eq. (39)) and success probability (lower panel) plotted vs the noise parameter $q_r \in [0, 1]$ for *depolarizing channel* (see Eq. (5)) with $n = 0, 1, 2, 3$ ancillary system (see the legend). Dots represent the numerical results, solid lines are used to denote the analytical results from Eqs. (23), (53).

II). Second, it depends on the parameters θ_{ij} , ϕ_{ij} determining the measurement settings in Alice's and Bob's laboratories. In view of this, we consider two different optimization problems. The first problem is to find the optimal choice of unitary that maximizes the Bell functional for given values of θ_{ij} , ϕ_{ij} :

$$\beta_n^{fix} = \max_U \mathcal{B}_n. \quad (39)$$

The second optimization problem includes the maximization over the choice of the measurement setting angles:

$$\beta_n^{opt} = \max_{U, \theta_{ij}, \phi_{ij}} \mathcal{B}_n. \quad (40)$$

For the estimation of β_n^{fix} we use, for the angles θ_{ij} , ϕ_{ij} , the values that maximize the CHSH functional when there is no ancilla and no error mitigation is applied. For the initial, noiseless state $|\Phi^+\rangle$, and for the case of

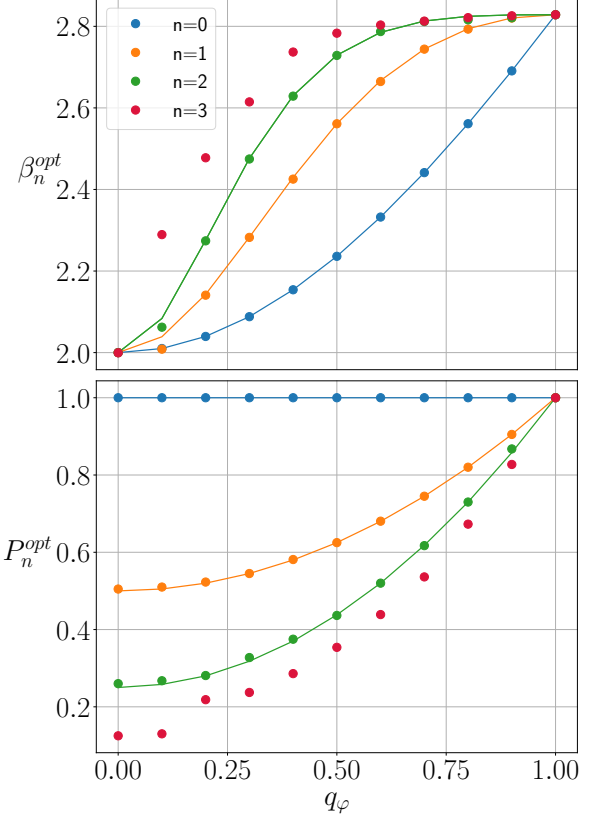


FIG. 12. Optimal CHSH value (top panel) optimizing also on the measurement settings (see Eq. (40)) and successful probability P_s (lower panels), plotted vs the noise parameter $q_\varphi \in [0.5, 1]$ for *dephasing channel*. Dots are for numerical optimization, solid lines for the ansatz unitary, for $n = 0, 1, 2, 3$ ancillary qubits.

depolarizing channel, these values are

$$(\phi_{0,0}, \theta_{0,0}) = (0, 0), \quad (41)$$

$$(\phi_{0,1}, \theta_{0,1}) = \left(0, \frac{\pi}{2}\right), \quad (42)$$

$$(\phi_{1,0}, \theta_{1,0}) = \left(0, \frac{\pi}{4}\right), \quad (43)$$

$$(\phi_{1,1}, \theta_{1,1}) = \left(\pi, \frac{\pi}{4}\right). \quad (44)$$

Similarly, the optimal settings for dephasing noise with parameter q_φ are obtained for

$$(\phi_{0,0}, \theta_{0,0}) = (0, 0), \quad (45)$$

$$(\phi_{0,1}, \theta_{0,1}) = \left(0, \frac{\pi}{2}\right), \quad (46)$$

$$(\phi_{1,0}, \theta_{1,0}) = (0, \arctan q_\varphi), \quad (47)$$

$$(\phi_{1,1}, \theta_{1,1}) = (\pi, \arctan q_\varphi). \quad (48)$$

Using these optimal settings, we obtain the maximum value of the Bell functional without error mitigation [59]:

$$\beta_0^{fix}(q_\varphi) = 2\sqrt{1 + q_\varphi^2}, \quad (49)$$

$$\beta_0^{fix}(q_r) = 2\sqrt{2} q_r, \quad (50)$$

respectively for dephasing and depolarizing noise. Based on the Conjectures 1 and 2, we derive the following analytical expressions for dephasing noise,

$$\beta_1^{\text{fix}}(q_\varphi) = \frac{6q_\varphi^2 + 2}{(q_\varphi^2 + 1)^{3/2}}, \quad (51)$$

$$\beta_2^{\text{fix}}(q_\varphi) = \frac{2(1 + 6q_\varphi^2 + q_\varphi^4)}{(1 + 3q_\varphi^2)\sqrt{1 + q_\varphi^2}}. \quad (52)$$

These values match the results of the numerical optimization. The associated success probabilities are as in Eqs. (20) and (27).

Similarly, using the ansatz unitary for $n = 1$ ancilla, we obtained the following result for mitigation of depolarizing noise:

$$\beta_1^{\text{fix}}(q_r) = 2\sqrt{2} q_r \frac{1 + q_r}{1 + q_r^2}, \quad (53)$$

which also match the numerical optimization, with success probability as in Eq. (23). For the case of two ancillas, our ansatz for the two-qubit unitaries does not match the numerical results.

Our results from the numerical optimization, for each approach, are shown in Fig. 10 and 12 following error mitigation with $n = 1, 2, 3$ ancillary qubits. The figures also show the figures of merit obtained from the encoding unitary ansatz, which match the numerical ones up to numerical precision.

Finally, we compute the optimized Bell functional including the optimization over the measurement settings, as defined in Eq. (40). For dephasing noise, we find that the Bell functional can be further improved by optimizing over the angles defining the measurement settings. This is shown in Fig. 12 together with the matching values obtained using our ansatz for the unitary encoding with one and two ancillas. By contrast, in case of depolarizing noise, optimization of the measurement setting does not improve the Bell functional above the classical threshold $\mathcal{B} = 2$. We argue that this is due to the higher symmetry of depolarizing noise with respect to dephasing.

E. Quantum metrology

Metrology is the scientific study of the measurement process, in its experimental and theoretical aspects. Loosely speaking, quantum metrology is the branch that focuses on measuring quantum states of matter or fields, potentially using quantum devices and, in certain settings, achieving levels of precision beyond what is possible classically [39, 60].

The Quantum Fisher Information (QFI) is often used within quantum metrology as a figure of merit that quantifies the amount of information that a family of quantum states ρ_θ carries about a parameter θ (e.g. the phase shift in an interferometer, the strength of a magnetic field)

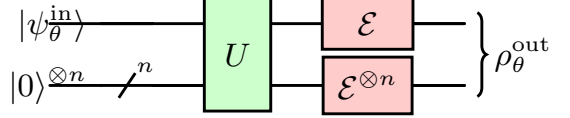


FIG. 13. The figure represents the application of the error mitigation scheme in the context of parameter estimation. We begin with the initial state $|\psi(\theta)\rangle = \cos(\theta/2)|0\rangle + \sin(\theta/2)|1\rangle$ for the signal qubit, where θ is the parameter to be estimated. Error mitigation is supported by n ancillary qubits prepared in the state $|0\rangle^{\otimes n}$ and an encoding unitary U . Signal and ancillary qubits are encoded before they experience the local noisy channel \mathcal{E} . Note that in this setup we do not post-select over the ancillary qubits (this would artificially reduce the number of useful measurements to estimate θ). Also, we do not apply the inverse unitary operation, since the QFI is invariant under unitary transformations.

that is to be measured. Formally, the QFI reads

$$Q = \text{Tr}(L^2 \rho_\theta), \quad (54)$$

where L is the symmetric logarithmic derivative [39, 61],

$$L = \sum_{n,m:p_n+p_m \neq 0} \frac{2 \langle e_m | \partial_\theta \rho | e_n \rangle}{\lambda_n + \lambda_m} |e_m\rangle \langle e_n|, \quad (55)$$

which is computed from the θ -dependent spectral decomposition

$$\rho_\theta = \sum_m \lambda_m |e_m\rangle \langle e_m|, \quad (56)$$

and depends on the derivative $\partial_\theta \rho$ of the density matrix with respect to the parameter θ .

The operational interpretation of the QFI is of particular interest in quantum metrology, as it quantifies the minimum statistical error attainable in the estimation of the parameter θ from N identical copies ρ_θ^N . According to the quantum Cramér-Rao bound [39, 61], the statistical error $\Delta\theta$ is bounded from below as follows:

$$\Delta\theta \geq (N Q)^{-1/2}. \quad (57)$$

Therefore, the QFI quantifies the sensitivity of the state to small changes in the parameter θ , thereby setting a limit to the precision with which θ can be estimated.

Our model is schematically depicted in Fig. 13. The parameter θ is initially encoded in the phase of a family of one-qubit pure states,

$$|\psi_\theta^{\text{in}}\rangle = e^{-i\theta\sigma_y/2}|0\rangle = \cos(\theta/2)|0\rangle + \sin(\theta/2)|1\rangle. \quad (58)$$

If such a state is measured without noise, it is easy to check that the associated QFI is $Q = 1$. Otherwise, if the state is subject to noise, the QFI is degraded, corresponding to the fact that the estimation of the parameter θ comes with greater uncertainty. For example, under depolarizing noise with parameter q_r , the above state maps to

$$\rho_\theta = \mathcal{E}(|\psi_\theta^{\text{in}}\rangle \langle \psi_\theta^{\text{in}}|), \quad (59)$$

and the QFI reads

$$Q_0(q_r) = q_r^2. \quad (60)$$

Our goal is to improve on this value by employing the error mitigation scheme. In the framework of quantum metrology, we apply a few modification to our scheme. First, we note that the QFI bounds the inverse of variance $\Delta\theta^2$ divided by the total number of measurements N . In this context, post-selection on the ancillary qubits would artificially reduce the effective value of N . Therefore, even if the post-selected QFI is augmented, this does not necessarily mean that the variance is made smaller. For this reason, as shown in Fig. 13, in this setup we do not post-select on the ancillary qubits. The second modification follows from the fact that the QFI is invariant under unitary transformations, i.e., in Eq. (54) the QFI does not change if we replace ρ_θ with $U^\dagger \rho_\theta U$, as long as U is independent of θ . Because of this, we do not need to apply the decoding unitary U^\dagger . Coming back to Fig. 13, the error-mitigated QFI is computed on the state ρ_θ^{out} , which includes both signal and ancillary qubits.

We have numerically computed the optimized QFI under depolarizing noise after application of error-mitigation with $n = 1, 2, 3$ ancillary qubits. The results of the numerical optimization are shown in Fig. 14, where for $n = 1, 2$ we also compare with the matching value obtained using the ansatz in Section III C for the encoding unitary in the case of one ancillary qubit:

$$Q_1(q_r) = \frac{2q_r^2}{q_r^2 + 1}. \quad (61)$$

We conclude with a remark. For the case of dephasing noise, the mitigation scheme works perfectly (i.e. it yields $Q = 1$) even without any ancillary qubits. To see this, note that the parameter θ in Eq. (58) represents a phase shift around σ_y . If the dephasing channel, as in Eq. (1), acts in the σ_z direction, the latter does not affect the ability of estimating θ , yielding $Q = 1$. Otherwise, the QFI may degrade if the dephasing is in the σ_y direction. However, in this latter case it is sufficient to apply a one-qubit rotation to map σ_y into σ_z to once again obtain $Q = 1$.

IV. CONCLUSIONS

Hardware-based approaches to achieve error mitigation have been developed recently [29–33], also in relation to applications of the phenomenon of error filtration, where local random errors are filtered out by exploiting constructive and destructive interference [27, 28].

Previous works have explored, either in the framework of optical modes or in the context of qubits, examples of schemes that achieved error filtration. Those scheme were based on a particular encoding and decoding of quantum information, e.g. via quantum Fourier transform [29, 30], by superposition of paths [31] or causal orders [32].

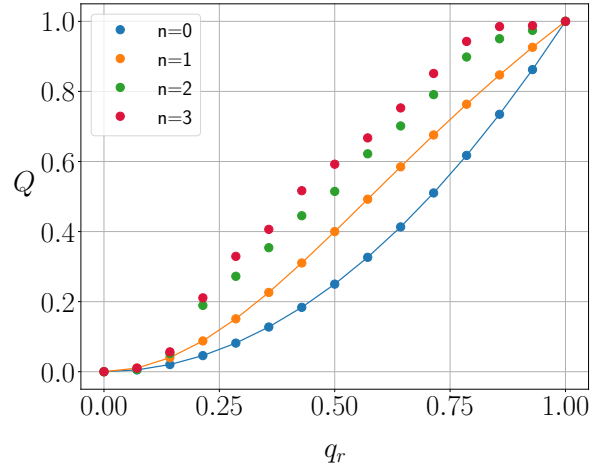


FIG. 14. The plot shows the optimal value of QFI optimized over all encoding unitary with $n = 0, 1, 2, 3$ ancillary qubits. The QFI is plotted vs the noise parameter of the depolarizing channel, see Eq. (4).

Here we have followed a different approach with the goal of determining the optimal encoding unitary, i.e. the quantum circuit of $n + 1$ qubits that optimally exploits interference to mitigate errors, for example, those arising from dephasing and depolarization. To achieve this goal, we have parameterized a generic unitary using the Shannon decomposition and numerically determined the optimal one, following the maximization of a suitable figure of merit. The choice of different figures of merit reflects different use cases for quantum information processing, from general computing to violation of Bell inequalities and quantum metrology. In some cases, the numerical optimization matches an analytical form for the figures of merit that we have obtained from a conjecture about the form of the optimal encoding rule.

Our model assumes that all the qubits, signals and ancillas, are subject to independent and identically distributed noise. This improves on previous works [32, 33], where the error mitigation scheme was not robust to errors in the ancillary qubits. In general, a hierarchy of errors may be introduced, where the ancillas are less noisy than the signal [31]. One more innovation of our work is that our scheme yields non-trivial error filtration also with just one ancillary qubit. In contrast, previous schemes needed at least two qubits (one control and one ancilla) to mitigate errors on a single qubit. However, we also assume that the encoding and decoding unitaries are error-free. This represents a limitation as in practice we expect that these pre and post-processing transformations will also be affected by noise. This is true, especially with an increasing number of ancillas. This observation paves the way for a research question to understand our scheme's robustness in the presence of imperfection in the encoding and decoding unitaries.

ACKNOWLEDGMENTS

We thank D. Pomarico for introducing us HTCondor, D. Amaro-Alcalá, F. Shahbeigi, R. Demkowicz-Dobrski, and E. Galvão for fruitful discussions.

This work has received funding from the European Union — Next Generation EU, through PNRR MUR project CN00000013 ‘Italian National Centre on HPC, Big Data and Quantum Computing’, PNRR MUR project PE0000023-NQSTI ‘National Quantum Science and Technology Institute’, and INFN through the project “QUANTUM”.

[1] M. A. Nielsen and I. L. Chuang, *Quantum computation and quantum information* (Cambridge university press, 2010).

[2] P. W. Shor (Ieee, 1994) pp. 124–134.

[3] L. K. Grover (Association for Computing Machinery, New York, NY, USA, 1996) p. 212–219.

[4] S. Aaronson and A. Arkhipov, *Theory of Computing* **9**, 143 (2013).

[5] S. McArdle, S. Endo, A. Aspuru-Guzik, S. C. Benjamin, and X. Yuan, *Rev. Mod. Phys.* **92**, 015003 (2020).

[6] M. C. Bañuls, R. Blatt, J. Catani, A. Celi, J. I. Cirac, M. Dalmonte, L. Fallani, K. Jansen, M. Lewenstein, S. Montangero, C. A. Muschik, B. Reznik, E. Rico, L. Tagliacozzo, K. V. Acoleyen, F. Verstraete, U.-J. Wiese, M. Wingate, J. Zakrzewski, and P. Zoller, *Eur. Phys. J. D* **74**, 165 (2020).

[7] A. Di Meglio, K. Jansen, I. Tavernelli, C. Alexandrou, S. Arunachalam, C. W. Bauer, K. Borrás, S. Carrazza, A. Crippa, V. Croft, *et al.*, arXiv preprint arXiv:2307.03236 (2023).

[8] C. L. Degen, F. Reinhard, and P. Cappellaro, *Reviews of modern physics* **89**, 035002 (2017).

[9] A. N. Boto, P. Kok, D. S. Abrams, S. L. Braunstein, C. P. Williams, and J. P. Dowling, *Phys. Rev. Lett.* **85**, 2733 (2000).

[10] J. P. Dowling, *Contemporary Physics* **49**, 125 (2008), <https://doi.org/10.1080/00107510802091298>.

[11] D. Gottesman, T. Jennewein, and S. Croke, *Phys. Rev. Lett.* **109**, 070503 (2012).

[12] F. V. Pepe, G. Scala, G. Chilleri, D. Triggiani, Y.-H. Kim, and V. Tamma, *The European Physical Journal Plus* **137**, 1 (2022).

[13] M. Tsang, R. Nair, and X.-M. Lu, *Phys. Rev. X* **6**, 031033 (2016).

[14] A. K. Ekert, *Phys. Rev. Lett.* **67**, 661 (1991).

[15] J. Barrett, L. Hardy, and A. Kent, *Physical Review Letters* **95**, 010503 (2005).

[16] A. Acín, N. Brunner, N. Gisin, S. Massar, S. Pironio, and V. Scarani, *Phys. Rev. Lett.* **98**, 230501 (2007).

[17] I. W. Primaatmaja, K. T. Goh, E. Y.-Z. Tan, J. T.-F. Khoo, S. Ghorai, and C. C.-W. Lim, *Quantum* **7**, 932 (2023).

[18] V. Zapatero, T. van Leent, R. Arnon-Friedman, W.-Z. Liu, Q. Zhang, H. Weinfurter, and M. Curty, *npj Quantum Information* **9**, 10.1038/s41534-023-00684-x (2023).

[19] J. Preskill, *Quantum* **2**, 79 (2018).

[20] S. Endo, S. C. Benjamin, and Y. Li, *Physical Review X* **8**, 031027 (2018).

[21] A. Strikis, D. Qin, Y. Chen, S. C. Benjamin, and Y. Li, *PRX Quantum* **2**, 040330 (2021).

[22] Z. Cai, R. Babbush, S. C. Benjamin, S. Endo, W. J. Huggins, Y. Li, J. R. McClean, and T. E. O’Brien, *Reviews of Modern Physics* **95**, 045005 (2023).

[23] S. Endo, Z. Cai, S. C. Benjamin, and X. Yuan, *Journal of the Physical Society of Japan* **90**, 032001 (2021).

[24] Y. Suzuki, S. Endo, K. Fujii, and Y. Tokunaga, *PRX Quantum* **3**, 010345 (2022).

[25] G. Acampora, M. Grossi, and A. Vitiello, in *2021 IEEE congress on evolutionary computation (CEC)* (IEEE, 2021) pp. 1826–1832.

[26] M. Lostaglio and A. Ciani, *Physical review letters* **127**, 200506 (2021).

[27] N. Gisin, N. Linden, S. Massar, and S. Popescu, *Phys. Rev. A* **72**, 012338 (2005).

[28] L.-P. Lamoureux, E. Brainis, N. J. Cerf, P. Emplit, M. Haelterman, and S. Massar, *Phys. Rev. Lett.* **94**, 230501 (2005).

[29] M. K. Vijayan, A. P. Lund, and P. P. Rohde, *Quantum* **4**, 303 (2020).

[30] C. Lupo and Z. Huang, arXiv preprint quant-ph/2310.01083 (2023).

[31] G. Lee, C. T. Hann, S. Puri, S. Girvin, and L. Jiang, *Physical Review Letters* **131**, 190601 (2023).

[32] J. Miguel-Ramiro, Z. Shi, L. Dellantonio, A. Chan, C. A. Muschik, and W. Dür, *Phys. Rev. Lett.* **131**, 230601 (2023).

[33] J. Miguel-Ramiro, Z. Shi, L. Dellantonio, A. Chan, C. A. Muschik, and W. Dür, *Phys. Rev. A* **108**, 062604 (2023).

[34] N. Brunner, D. Cavalcanti, S. Pironio, V. Scarani, and S. Wehner, *Reviews of Modern Physics* **86**, 419 (2014).

[35] V. Scarani, *Bell Nonlocality* (Oxford University Press, 2019).

[36] F. Xu, X. Ma, Q. Zhang, H.-K. Lo, and J.-W. Pan, *Reviews of Modern Physics* **92**, 10.1103/revmodphys.92.025002 (2020).

[37] C. Portmann and R. Renner, *Reviews of Modern Physics* **94**, 025008 (2022).

[38] N. Gigena, E. Panwar, G. Scala, M. Araújo, M. Farkas, and A. Chaturvedi, arXiv preprint arXiv:2405.08743 (2024).

[39] J. S. Sidhu and P. Kok, *AVS Quantum Science* **2**, 014701 (2020), https://pubs.aip.org/avs/aqs/article-pdf/doi/10.1116/1.5119961/16700179/014701_1_online.pdf.

[40] M. Möttönen and J. J. Vartiainen, *Trends in Quantum Computing Research*, 149 (2006).

[41] F. S. Khan and M. Perkowski, arXiv preprint quant-ph/0511041 (2005).

[42] A. M. Krol, A. Sarkar, I. Ashraf, Z. Al-Ars, and K. Berthels, *Applied Sciences* **12**, 759 (2022).

[43] A. Barenco, C. H. Bennett, R. Cleve, D. P. DiVincenzo, N. Margolus, P. Shor, T. Sleator, J. A. Smolin, and H. Weinfurter, *Physical review A* **52**, 3457 (1995).

[44] S. Bullock and I. Markov, *Phys. Rev. A* **68**, 012318 (2003).

[45] G. Cybenko, Computing in science & engineering **3**, 27 (2001).

[46] M. Möttönen, J. J. Vartiainen, V. Bergholm, and M. M. Salomaa, Physical review letters **93**, 130502 (2004).

[47] C. C. Paige and M. Wei, Linear Algebra and its Applications **208**, 303 (1994).

[48] J. J. Vartiainen, M. Möttönen, and M. M. Salomaa, Physical review letters **92**, 177902 (2004).

[49] V. V. Shende, I. L. Markov, and S. S. Bullock, Physical Review A **69**, 062321 (2004).

[50] V. V. Shende, S. S. Bullock, and I. L. Markov, Proceedings of the 2005 Asia and South Pacific Design Automation Conference ASP-DAC '05, 272–275 (2005).

[51] V. Bergholm, J. Izaac, M. Schuld, C. Gogolin, S. Ahmed, V. Ajith, M. S. Alam, G. Alonso-Linaje, B. AkashNarayanan, A. Asadi, *et al.*, arXiv preprint arXiv:1811.04968 (2018).

[52] D. P. Nadlinger, P. Drmota, B. C. Nichol, G. Araneda, D. Main, R. Srinivas, D. M. Lucas, C. J. Ballance, K. Ivanov, E. Y.-Z. Tan, P. Sekatski, R. L. Urbanke, R. Renner, N. Sangouard, and J.-D. Bancal, Nature **607**, 682 (2022).

[53] W.-Z. Liu, Y.-Z. Zhang, Y.-Z. Zhen, M.-H. Li, Y. Liu, J. Fan, F. Xu, Q. Zhang, and J.-W. Pan, Physical Review Letters **129**, 050502 (2022).

[54] W. Zhang, T. van Leent, K. Redeker, R. Garthoff, R. Schwonnek, F. Fertig, S. Eppelt, W. Rosenfeld, V. Scarani, C. C.-W. Lim, and H. Weinfurter, Nature **607**, 687 (2022).

[55] J. S. Bell, Physics Physique Fizika **1**, 195 (1964).

[56] J. F. Clauser, M. A. Horne, A. Shimony, and R. A. Holt, Physical Review Letters **23**, 880 (1969).

[57] B. S. Cirel'son, Letters in Mathematical Physics **4**, 93 (1980).

[58] A. Rico, M. B. Morán, F. Shahbeigi, and K. Życzkowski, arXiv preprint arXiv:2408.10317 (2024).

[59] R. Horodecki, P. Horodecki, and M. Horodecki, Physics Letters A **200**, 340 (1995).

[60] V. Giovannetti, S. Lloyd, and L. Maccone, Nature photonics **5**, 222 (2011).

[61] M. G. Paris, International Journal of Quantum Information **7**, 125 (2009).

Appendix A: Ansatz for the encoding unitary with one ancilla

Consider the following encoding unitary, which maps the computational basis into the Bell basis:

$$U = \sum_{j,k=0,1} |\Phi_{jk}\rangle\langle jk|, \quad (\text{A1})$$

where Φ_{jk} denote the Bell states. The inverse unitary is

$$U^\dagger = \sum_{j,k=0,1} |jk\rangle\langle\Phi_{jk}|. \quad (\text{A2})$$

To compute the entanglement fidelity, we start with the state (with ancilla initialized in $|0\rangle$)

$$\xrightarrow{\frac{1}{\sqrt{2}}} (|0\rangle_R|0\rangle_S|0\rangle_A + |1\rangle_R|1\rangle_S|0\rangle_A). \quad (\text{A3})$$

Applying the encoding unitary to this state we obtain

$$\xrightarrow{\frac{1}{\sqrt{2}}} (|0\rangle_R|\Phi_{00}\rangle_{SA} + |1\rangle_R|\Phi_{10}\rangle_{SA}). \quad (\text{A4})$$

If the local noise is described as a Pauli channel, then it can be viewed as the application of random Pauli unitaries. Let V_1 be the Pauli unitary applied on qubit S and V_2 the one applied on qubit A . For a given realization of the noise, the above state becomes

$$\xrightarrow{\frac{1}{\sqrt{2}}} (|0\rangle_R(V_1 \otimes V_2)|\Phi_{00}\rangle_{SA} + |1\rangle_R(V_1 \otimes V_2)|\Phi_{10}\rangle_{SA}). \quad (\text{A5})$$

After the noise is applied, it is time to apply the inverse unitary, yielding

$$\begin{aligned} \xrightarrow{U^\dagger} & \sum_{jk} \frac{1}{\sqrt{2}} (|0\rangle_R|jk\rangle\langle\Phi_{jk}|(V_1 \otimes V_2)|\Phi_{00}\rangle_{SA} \\ & + |1\rangle_R|jk\rangle\langle\Phi_{jk}|(V_1 \otimes V_2)|\Phi_{10}\rangle_{SA}). \end{aligned} \quad (\text{A6})$$

Since we post-selected on the ancillary qubit being in the state $|0\rangle$, of the above state we only need to consider the terms with $k = 0$. The resulting, non-normalized state is

$$\begin{aligned} |\psi_{V_1, V_2}\rangle = & \frac{1}{\sqrt{2}} \sum_j |0\rangle_R|j\rangle\langle\Phi_{j0}|(V_1 \otimes V_2)|\Phi_{00}\rangle_{SA} \\ & + |1\rangle_R|j\rangle\langle\Phi_{j0}|(V_1 \otimes V_2)|\Phi_{10}\rangle_{SA}. \end{aligned} \quad (\text{A7})$$

From this we obtain the success probability after averaging the quantity $\langle|\psi_{V_1, V_2}||\psi_{V_1, V_2}\rangle$ over the random Pauli unitaries:

$$P_1 = \frac{1}{2} \sum_{V_1, V_2} \pi(V_1)\pi(V_2) \sum_j \left(|\langle\Phi_{j0}|V_1 \otimes V_2|\Phi_{00}\rangle|^2 |\langle\Phi_{j0}|V_1 \otimes V_2|\Phi_{10}\rangle|^2 \right) \quad (\text{A8})$$

$$= \frac{1}{2} \sum_{V_1, V_2} \pi(V_1)\pi(V_2) \left(|\langle\Phi_{00}|V_1 \otimes V_2|\Phi_{00}\rangle|^2 + |\langle\Phi_{10}|V_1 \otimes V_2|\Phi_{00}\rangle|^2 + |\langle\Phi_{00}|V_1 \otimes V_2|\Phi_{10}\rangle|^2 + |\langle\Phi_{10}|V_1 \otimes V_2|\Phi_{10}\rangle|^2 \right), \quad (\text{A9})$$

where $\pi(V)$ is the probability of the Pauli unitary V .

For the case of depolarizing channel, the three Pauli errors have the same probability, equal to $(1 - p_r)/3$. This symmetry implies

$$P_1(q_r) = \sum_{V_1, V_2} \pi(V_1)\pi(V_2) \left(|\langle \Phi_{00}|V_1 \otimes V_2|\Phi_{00}\rangle|^2 + |\langle \Phi_{10}|V_1 \otimes V_2|\Phi_{00}\rangle|^2 \right) \quad (\text{A10})$$

$$= p_r^2 + \frac{(1 - p_r)^2}{3} + 2p_r \frac{1 - p_r}{3} + 2 \frac{(1 - p_r)^2}{9} \quad (\text{A11})$$

$$= \frac{5 - 4p_r + 8p_r^2}{9} = \frac{1 + q_r^2}{2}. \quad (\text{A12})$$

The un-normalized fidelity is obtained by taking the average of the quantity $|\langle \Phi^+|\psi_{V_1, V_2}\rangle|^2$,

$$\sum_{V_1, V_2} \pi(V_1)\pi(V_2) |\langle \Phi^+|\psi\rangle|^2 = \frac{1}{4} \sum_{V_1, V_2} \pi(V_1)\pi(V_2) |\langle \Phi_{00}|V_1 \otimes V_2|\Phi_{00}\rangle + \langle \Phi_{10}|V_1 \otimes V_2|\Phi_{10}\rangle|^2. \quad (\text{A13})$$

Note that each term $\langle \Phi_{00}|V_1 \otimes V_2|\Phi_{00}\rangle$ and $\langle \Phi_{10}|V_1 \otimes V_2|\Phi_{10}\rangle$ is non-zero only if $V_1 = V_2$. Therefore, the non-normalized fidelity reads

$$\frac{1}{4} \sum_V \pi(V)^2 |\langle \Phi_{00}|V \otimes V|\Phi_{00}\rangle + \langle \Phi_{10}|V \otimes V|\Phi_{10}\rangle|^2. \quad (\text{A14})$$

Also note $\langle \Phi_{00}|V \otimes V|\Phi_{00}\rangle = \pm 1$ as well as $\langle \Phi_{10}|V \otimes V|\Phi_{10}\rangle = \pm 1$, but they have the same sign only if $V = \sigma_0$ or $V = \sigma_y$ ². Finally we obtain the following value for the non-normalized fidelity:

$$\sum_{V=\sigma_0, \sigma_2} p(V)^2 = p_r^2 + \left(\frac{1 - p_r}{3} \right)^2 = \frac{1 + 2q_r + 5q_r^2}{8}. \quad (\text{A15})$$

Computing the (normalized) fidelity we obtain the result presented in Eq. (24),

$$\mathcal{F}_1(q_r) = \frac{1}{4} \frac{1 + 2q_r + 5q_r^2}{1 + q_r^2}. \quad (\text{A16})$$

Appendix B: Ansatz for the encoding unitary with two ancillas

The encoding rule in Eqs. (25)-(26) can be obtained from different choices of the encoding unitary U . One possible choice is a unitary that is isomorphic to the direct sum of two four-dimensional quantum Fourier transform. In the three-qubit computational basis $\{|0\rangle_S|00\rangle_A, |0\rangle_S|01\rangle_A, |0\rangle_S|10\rangle_A, |0\rangle_S|11\rangle_A, |1\rangle_S|00\rangle_A, |1\rangle_S|01\rangle_A, |1\rangle_S|10\rangle_A, |1\rangle_S|11\rangle_A\}$, this is represented by the unitary matrix

$$U = \frac{1}{2} \begin{pmatrix} 1 & 0 & 0 & 1 & 0 & 1 & 1 & 0 \\ 0 & 1 & -1 & 0 & 1 & 0 & 0 & -1 \\ 0 & 1 & -i & 0 & -1 & 0 & 0 & i \\ 1 & 0 & 0 & i & 0 & -1 & -i & 0 \\ 0 & 1 & 1 & 0 & 1 & 0 & 0 & 1 \\ 1 & 0 & 0 & -1 & 0 & 1 & -1 & 0 \\ 1 & 0 & 0 & -i & 0 & -1 & i & 0 \\ 0 & 1 & i & 0 & -1 & 0 & 0 & -i \end{pmatrix}. \quad (\text{B1})$$

Note that this matrix implements a quantum Fourier transform in each subspace of given parity.

² The Pauli unitary here is σ_2 because of our choice of the encoding into Bell states. For a different we may have a different Pauli

error, but only one Pauli error can yield the same sign on both the terms.

Let us consider the application of this encoding rule to mitigate dephasing noise. We start from the entangled state $|\Phi^+\rangle_{RS}|00\rangle_A$ between reference and system qubit, then apply the encoding unitary to the system and ancillary qubits:

$$|\Phi^+\rangle_{RS}|00\rangle_A = \frac{1}{\sqrt{2}} (|00\rangle_{RS}|00\rangle_A + |11\rangle_{RS}|00\rangle_A) \quad (\text{B2})$$

$$\xrightarrow{U} \frac{1}{\sqrt{2}} \left(|0\rangle_R \frac{|000\rangle + |011\rangle + |101\rangle + |110\rangle}{2} + |1\rangle_R \frac{|001\rangle + |010\rangle + |100\rangle + |111\rangle}{2} \right). \quad (\text{B3})$$

As done in Section III C we apply a local random phase to each qubit (except the reference). A given realization of the noise yields

$$\frac{1}{\sqrt{2}} \left(|0\rangle_R \frac{|000\rangle + e^{i\theta_2+i\theta_3}|011\rangle + e^{i\theta_1+i\theta_3}|101\rangle + e^{i\theta_1+i\theta_2}|110\rangle}{2} + |1\rangle_R \frac{e^{i\theta_3}|001\rangle + e^{i\theta_2}|010\rangle + e^{i\theta_1}|100\rangle + e^{i\theta_1+i\theta_2+i\theta_3}|111\rangle}{2} \right). \quad (\text{B4})$$

Applying the inverse unitary and after post-selection on the ancillary qubit, we obtain the non-normalized state

$$|\psi_{\theta_1, \theta_2, \theta_3, \theta_4}\rangle = \frac{1}{\sqrt{2}} \left(|0\rangle_R |0\rangle_S \frac{1 + e^{i\theta_2+i\theta_3} + e^{i\theta_1+i\theta_3} + e^{i\theta_1+i\theta_2}}{4} + |1\rangle_R |1\rangle_S \frac{e^{i\theta_3} + e^{i\theta_2} + e^{i\theta_1} + e^{i\theta_1+i\theta_2+i\theta_3}}{2} \right). \quad (\text{B5})$$

First, the probability of successful post-selection is obtained from the average over noise realizations of

$$|\langle \psi_{\theta_1, \theta_2, \theta_3, \theta_4} | \psi_{\theta_1, \theta_2, \theta_3, \theta_4} \rangle|^2 = \frac{1}{2} \left| \frac{1 + e^{i\theta_2+i\theta_3} + e^{i\theta_1+i\theta_3} + e^{i\theta_1+i\theta_2}}{4} \right|^2 + \frac{1}{2} \left| \frac{e^{i\theta_3} + e^{i\theta_2} + e^{i\theta_1} + e^{i\theta_1+i\theta_2+i\theta_3}}{2} \right|^2. \quad (\text{B6})$$

From this we obtain

$$P_2(q_\varphi) = \frac{1 + 3q_\varphi^2}{4}. \quad (\text{B7})$$

Second, the non-normalized entanglement fidelity is obtained from the average over noise realization of

$$|\langle \Phi^+ | \psi_{\theta_1, \theta_2, \theta_3, \theta_4} \rangle|^2 = \left| \frac{e^{i\theta_3} + e^{i\theta_2} + e^{i\theta_1} + e^{i\theta_1+i\theta_2+i\theta_3} + e^{i\theta_3} + e^{i\theta_2} + e^{i\theta_1} + e^{i\theta_1+i\theta_2+i\theta_3}}{8} \right|^2. \quad (\text{B8})$$

From this we obtain the non-normalized fidelity

$$\left(\frac{1 + q_\varphi}{2} \right)^3. \quad (\text{B9})$$

Intuitively, a good encoding rule is such that the probability of success P_2 is minimized and the quantity not-normalized fidelity $P_2 \mathcal{F}_2$ is maximized. With the above choice we obtain

$$\mathcal{F}_2(q_\varphi) = \frac{(q_\varphi + 1)^3}{6q_\varphi^2 + 2}. \quad (\text{B10})$$
